THE JOURNAL OF PHYSICAL CHEMISTRY Letters

pubs.acs.org/JPCL

Nanowire−Quantum Dot Hybridized Cell for Harvesting Sound and Solar Energies

Minbaek Lee,† Rusen Yang,† Cheng Li, and Zhong Lin Wang*

School of Material Science and Engineering, Georgia Institute of Technology, Georgia 30332

ABSTRACT We have demonstrated sound-wave-driven nanogenerators using both laterally bonded single wires and vertically aligned nanowire arrays for energy harvesting in the frequency range of 35−1000 Hz. The electricity produced by the single wire generator (SWG) is linearly proportional to the input acoustic energy, while the frequency does not affect the performance of the SWG in this study. By infiltrating CdS/CdTe quantum dots among vertical nanowires, we have fabricated a hybrid cell that simultaneously harvests both sound and solar energies. This demonstrates a possible approach for effectively harvesting available energies in our living environment with and without the presence of light.

SECTION Energy Conversion and Storage

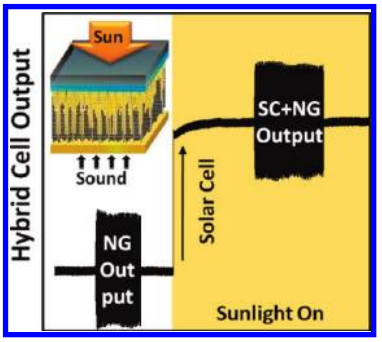

In addition to solar energy, enormous mechanical vibrational energy exists in our living environment with a large variation in amplitude and frequency, such as wind, sonic wave, hydraulic, and even noises. Harvesting this type of "random" energy can be a practical solution to power small mobile electronics for the future sensor network.[1,2] Great efforts have been made to efficiently convert solar, mechanical, and chemical energies into electricity,[3−5] but most of the technologies demonstrated are designed to harvest only one type of energy. As a future direction in energy research, simultaneous harvesting of multitype energy by a single device was first demonstrated for solar and mechanical energy[6] as well as chemical and mechanical energy,[7] which are referred to as hybrid energy cells.

Acoustic waves, such as various sound noises from any living activities, car traffic, and the construction industry, are one of the most common mechanical vibrations in our surroundings. As for indoor mobile electronics, other types of energies are of equal or even more importance than solar energy. It is important to develop technologies that simultaneously harvest multitype energies and use whatever is available. The previously demonstrated hybrid cell (HC) utilizes an ultrasonic wave with a fixed frequency of ∼41 kHz and irregular biomotion at ∼10 Hz or below.[6−10] Considering that, our living environment has abundant mechanical vibrations with various frequencies ranging from a few to thousands of Hz. A systematic study of the nanogenerator (NG) in various acoustic frequencies is needed for practical applications of the NG.

In this Letter, we first present the nanogenerators fabricated using both laterally bonded single wires and vertically aligned nanowire arrays for harvesting sound energy in the frequency range of 35−1000 Hz. The electricity produced by the single wire generator (SWG) is linearly proportional to the input acoustic energy, while the frequency does not affect the performance of the SWG in this study. Then, by infiltrating CdS/CdTe quantum dots[11] among vertical nanowires, we fabricated a "composite" type of HC that harvests both sound and solar energies in a complete single-volume layer rather than a stacked layer structure as we first demonstrated,[6] which is a promising approach for potential driving of portable electronics. This research is expected to inspire new research effort for developing the HC.

Lateral Single Wire Generator for Harvesting Sound Energy. Traditional piezoelectric generator is based on a two-layer bender (or bimorph)-mounted cantilever beam, which produces the maximum power when the driving frequency matches the resonance frequency of the cantilever.[12] In practice, a low-resonance-frequency resonator tends to have a large size/mass, which is too stiff to be driven by relatively weak sonic wave, while a small-size resonator has a high resonance frequency that is beyond the sonic wave frequency range, although it can be driven by small mechanical agitation. The cantilever-based piezoelectric generator is not the most effective choice for harvesting random sonic wave energy with a large variation in amplitude and frequency.

Recently, piezoelectric ZnO nanowires (NWs) have been shown to be effective for harvesting small-magnitude mechanical energy.[5,6,13−15] The SWG is based on a single piezoelectric ZnO wire with its two ends bonded to a flexible polymer substrate, as reported previously.[9] The ZnO wire is stretched or compressed when the substrate is bent upward and downward under external excitation. The thickness of the substrate is much larger than the diameter of the ZnO NW. Consequently, the ZnO NW experiences solely tensile strain or solely compressive strain, depending on the bending direction of the substrate. The strain within the piezoelectric NW thereafter produces a piezoelectric field along the length of

Received Date: August 23, 2010
Accepted Date: September 14, 2010
Published on Web Date: September 17, 2010

DOI: 10.1021/jz101195n | *J. Phys. Chem. Lett.* **2010**, *1*, 2929–2935

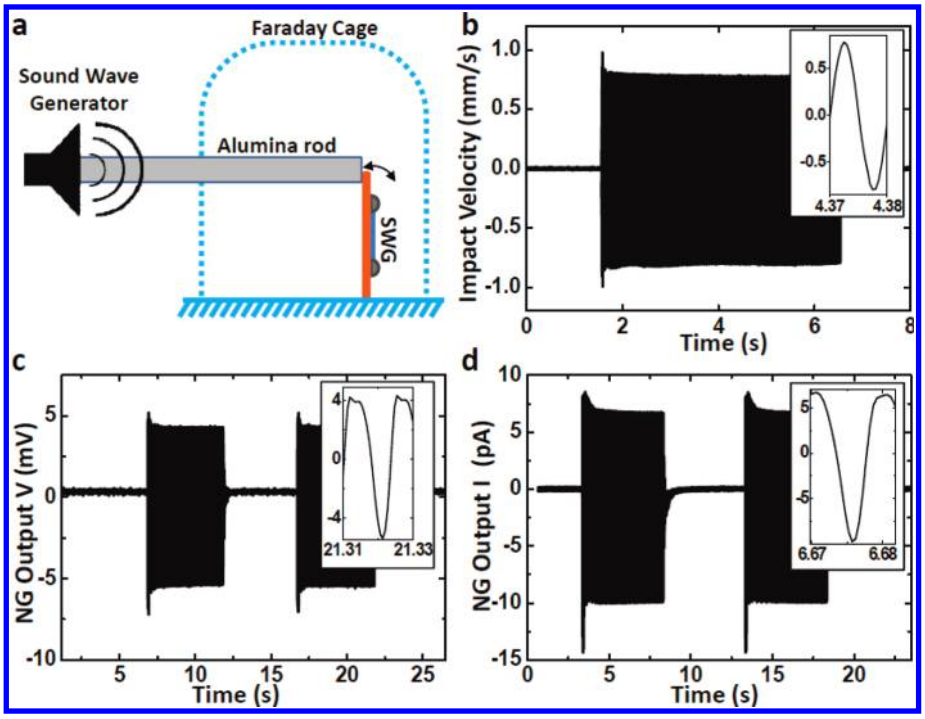

Figure 1. (a) Schematic diagram showing the experimental setup for driving a SWG using a sonic wave. (b) Impact velocity at the tip of the alumina rod at 100 Hz, showing the harmonic mechanical input to the nanogenerator. (c, d) Open-circuit voltage and the short-circuit current output from the SWG when it is triggered by a sound wave at 100 Hz. The inset is an enlarged plot of the output signal.

the NW. The free charge carriers in the external circuit are driven to flow by the piezoelectric potential difference across two ends of the stressed NW, while the Schottky contact at the interface can gate and regulate the current flow during the energy conversion process.[7,9−10] The mechanic−electric energy conversion of the NG relies on the transient current flow driven by the piezoelectric potential produced by the dynamic strain.

A sound transducer was employed to generate acoustic vibration at a desired frequency. An alumina rod was firmly attached to the sound wave generator at one end, and its other end was placed directly on the top of the substrate on which a SWG was mounted, as shown in Figure 1a. The sound wave generated by the transducer was directly transmitted to the SWG. A high-sensitivity accelerometer (Wilcoxon Research, Model 736) was used to characterize the sound transducer and measure the magnitude of the vibration. The vibration of the end surface of the alumina rod was measured with the accelerometer. Figure 1b presents the impact velocity of the beam derived from the accelerometer when the transducer is excited at a frequency of 100 Hz. The measurement of the accelerometer has a sinusoidal shape at a frequency of 100 Hz, which agrees well with the sinusoidal exciting signal input to the acoustic transducer. The measurement of the accelerometer indicates a harmonic vibration from the surface. The impact velocity is about 0.78 mm/sec at a frequency of 100 Hz, and the acoustic power is proportional to the square of the impact velocity.

Figure 1c and d present the open-circuit voltage and short-circuit current of the SWG driven by the acoustic vibration at 100 Hz. Figure 1c shows that the voltage output from the SWG reaches about ∼4 mV and the current reaches about ∼8 pA. The fluctuation of the signal at the early stage of the vibration was mainly caused by the instability of the transducer as well as the fluctuation of the substrate. The signal became very stable in a 1 s or less. Both the voltage and the current output from the SWG showed sinusoidal shapes, which is consistent to the harmonic vibration of the rod surface. In addition to the 100 Hz, different frequencies from 35 to 1000 Hz were systematically tested, and a similar result was also observed.

The sound transducer used in this experiment cannot remain at a fixed power output at a different excitation frequency. However, the power of the acoustic vibration is proportional to the impact velocity as induced by the transducer on the alumina rod, which can be derived from the accelerometer measurement. The measured NG output voltage divided by the impact velocity of the rod can be helpful to understand the performance of the NG at different frequencies, as illustrated in Figure 2a. The voltage output fluctuates much greater at lower frequency (<200 Hz) than that at high frequency (>200 Hz). This is mainly due to the fluctuation of the transducer at low frequency. Overall, the voltage output is relatively uniform over the entire frequency range under investigation. In other words, the voltage output does not significantly depend on the frequency of the acoustic vibration.

The relationship between the voltage output of the SWG and the impact velocity of the acoustic vibration at the end of the alumina rod is shown in Figure 2b. The relationship between the current output and the impact velocity of acoustic vibration is shown in Figure 2c. Although each data point corresponds to the measurement at different frequencies, the

DOI: 10.1021/jz101195n | J. Phys. Chem. Lett. 2010, 1, 2929–2935

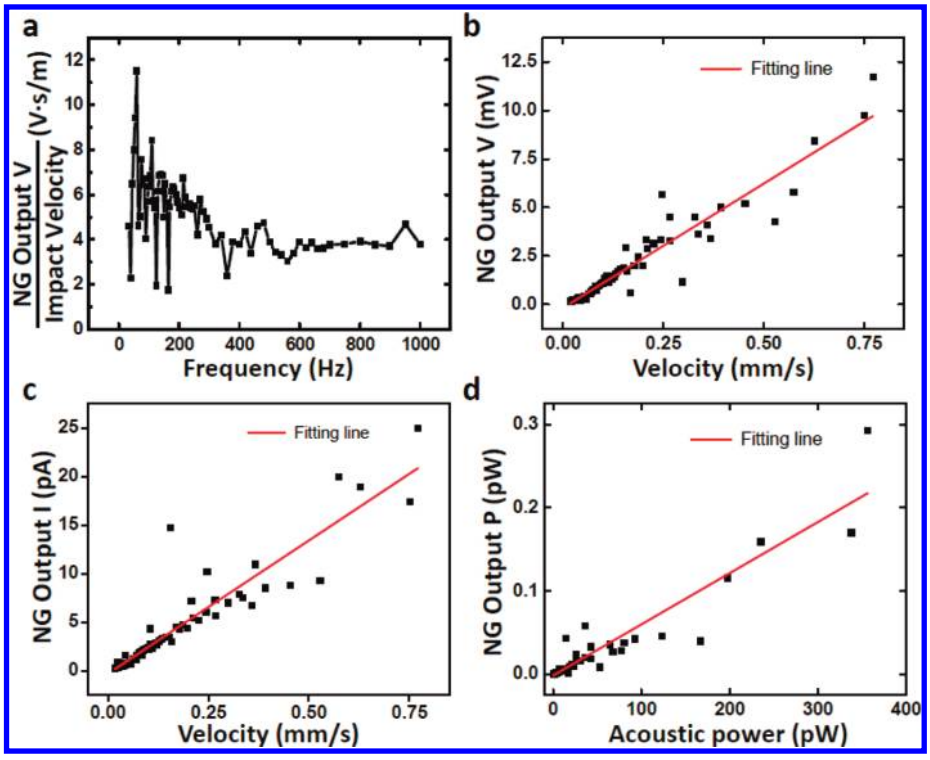

Figure 2. (a) Ratio of the SWG open-circuit voltage and the applied mechanical impact velocity as a function of the driving frequency. (b, c) Voltage and current output from the SWG which is driven by acoustic vibration at different impact velocity. (d) Electric power output from the SWG which is driven by acoustic vibration with different acoustic power.

linear relationship is clearly revealed. The electric energy output is estimated as $P_{electric} = V \cdot I$, and the acoustic power at the end surface of alumina rod is estimated to be $P_{acoustic} = Z \cdot v^2 \cdot A$, where V, I, Z, v, and A are the voltage output, current output, acoustic impedance (40.6×10^6 kg/(s·m^2) for alumina), impact velocity, and lateral cross section area of the ZnO wire, respectively. The ZnO wire is ~800 nm in diameter and ~100 μm in length. The acoustic power transferred to the ZnO wire is significantly decreased due to the damping effect of the substrate and the reflection and absorption at the interface. However, the plot of $P_{electric}$ versus $P_{acoustic}$ in Figure 2d can still qualitatively reveal the performance of the SWG. The acoustic power varies over several orders of magnitude at different frequencies. The linear relationship between the NG output electric power and the acoustic power is clearly demonstrated in Figure 2d. Consequently, the energy conversion can be realized over a wide range of frequencies and a wide range of stimuli magnitudes.

Hybrid Cell for Concurrent Harvesting of Sound and Solar Energies. The next step for us is to demonstrate that a HC simultaneously harvests sound and solar energies. For the sound-driven NG to be used as the basic structure of the HC, we used aligned nanowires because they are easy to integrated with the structure of the solar cell (SC). Our HC is based on a structure of vertical NW array integrated NG (VING) with the infiltration of QDs among the NW forest. The vertically aligned NWs are responsible for the harvesting of sound energy, and the CdS (n-type)/CdTe (p-type) nanoparticles are responsible for harvesting solar energy. The vertically aligned NWs were grown by a solution-based approach at low temperature.[16] The nanoparticles were infiltrated by the spin-casting method.[11] Both scanning electron microscopy (SEM) and transmission electron microscopy (TEM) images (see also Figure S2 in Supporting Information (SI)) clearly show the "composite" structure of the NWs and the QDs (Figure 3a and b). By the spin-casting method, we could obtain a relatively uniform QD layer, leaving the top end of ZnO NWs for the electric contact afterward (Figure 3b). To fabricate the bottom Au electrode, the RF sputtering method was implemented with the shadow mask technique (see the details in Experimental Methods in SI). Since our HC was composed of a pn-heterojunction of QDs and vertical NW arrays in contact with different metals such as ITO (top electrode) and Au (the bottom electrode), the $I-V$ curve was found to be asymmetric, with the lowest resistance of ~0.1 MΩ, as shown in Figure 3c.

We first investigated acoustic-driven output from the VING. By applying a sound wave, a periodic force produced a short-circuit current or an open-circuit voltage. Figure 3d presents the short-circuit current and open-circuit voltage of the VING driven by the acoustic vibration at a frequency of 50 Hz. It shows that the current output was from ~22 to 45 nA and the corresponding generated voltage was ~1.5−6.0 mV. VING also followed the frequency of 50 Hz (insets of Figure 3d), which is the same as those of the applied acoustic wave. The linear superposition of both the current and voltage was conducted to rule out any artificial signal output and to examine large-scale integration for a practical application.[17,18]

DOI: 10.1021/jz101195n | J. Phys. Chem. Lett. 2010, 1, 2929–2935

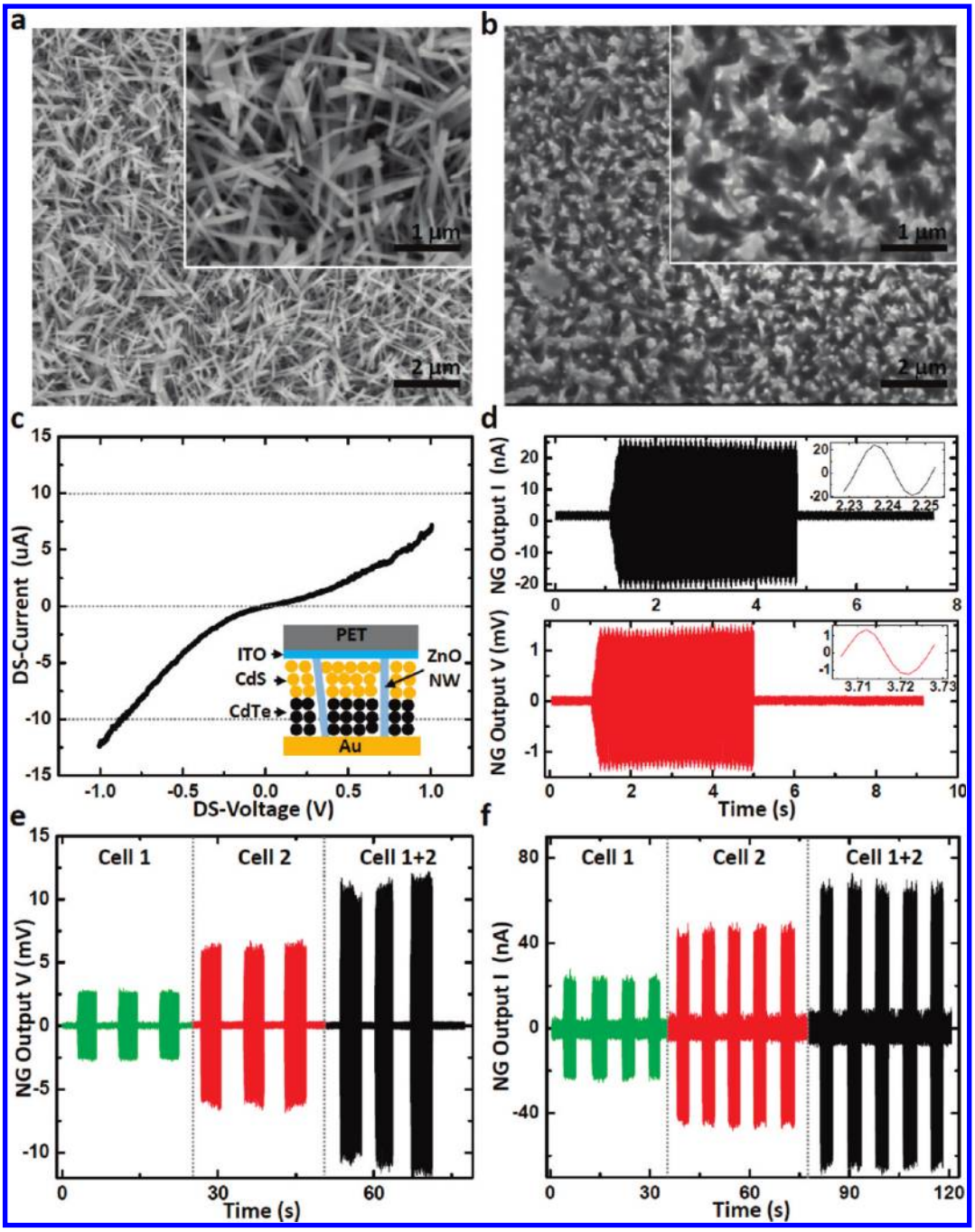

Figure 3. (a) Scanning electron microscopy image of the as-grown vertical ZnO NW array on a PET substrate with an ITO conductive layer. (b) Scanning electron microscope image of ZnO NWs after infiltrating with CdS/CdTe quantum dots. The clustering of the nanowires is likely due to the surface tension in spin coating. (c) $I-V$ characteristic of a hybrid device using ZnO nanowires and CdS/CdTe QDs, whose structure is shown in the inset. (d) Open-circuit voltage (bottom) and the short-circuit current (top) output from the VING when the acoustic wave is applied to the generator at a frequency of ~50 Hz. Insets show the details of generated wave shapes in current and voltage output. It matches well with acoustic vibration of the transducer. (e) Linear superposition test of open-circuit voltages in serial connection of two HCs. Cell 1 (green curve) and Cell 2 (red curve) show the peak-to-peak voltage outputs of ~3 and ~7 mV, respectively. In serial connection of Cell 1 and Cell 2, the peak-to-peak voltage output reaches ~10 mV. (f) Linear superposition test of short-circuit currents in parallel connection of two HCs. Cell 1 (green curve) and Cell 2 (red curve) show the peak-to-peak current outputs of ~25 nA and ~48 nA, respectively. In parallel connection of Cell 1 and Cell 2, the peak-to-peak current output reaches ~69 nA.

Since our hybrid devices with an average area of ~0.25 cm^2 can vibrate in the same phase under identical acoustic waves with areas of ~10 cm^2, we could observe the integrated current and voltage using two relatively small devices with areas of ~0.5 cm^2 in parallel and serial connections, respectively. In the case of voltage superposition, the voltage output

DOI: 10.1021/jz101195n | J. Phys. Chem. Lett. 2010, 1, 2929–2935

of each HC was measured individually under the same conditions; thereafter, each cell was connected in serial and tested again. Figure 3e shows the voltage outputs from our HC in individual and serial connection. Cell 1 and Cell 2 showed peak-to-peak NG output voltages V of ∼3 and ∼7 mV in the open circuit, respectively (Figure 3e, green and red curve). After the two generators were connected in serial, the peak-to-peak output voltage added up to an average of ∼10 mV (Figure 3e, black curve). Also, by connecting two individual cells in parallel, the output current exhibits a sum of the two cells (Figure 3f). A single sound generator of Cell 1 showed peak-to-peak NG output current I of ∼25 nA in a short circuit, and the sound generator of Cell 2 gave a peak-to-peak current I of ∼48 nA under the same acoustic wave. After two generators were connected in parallel, the peak-to-peak output current added up to an average of ∼69 nA (Figure 3f, black curve). On the basis of superposition of the voltage and current signal outputs using two devices, our device can generate resonant signal outputs capable of being added up as long as the acoustic source is large enough to excite any of those devices in a synchronized manner.

We also tested the concurrent-energy-harvesting performance of our composite HC under the both acoustic wave and simulated solar illumination. The schematic diagram of our hybrid device is shown in Figure 4a, depicting different incoming energy sources. Acoustic waves are applied to HC in the direction from the bottom Au electrode, while the light source illuminates the embedded pn-heterojunction based on CdS/CdTe QDs through the transparent PET layer (300 μm) with conductive ITO electrode (50 nm). All components that we need can be packaged in a single volume for efficient use of space.

For simplicity, we can assume that the HC has two individual generators in parallel, as shown in the band diagram in Figure 4b. SC and VING correspond to upper and lower diagrams, respectively. In the case of SC, it is supposed to generate direct current (DC) flow. Under sunlight illumination, the light passes through transparent upper structures of our HC as well as the CdS layer placed underneath (Figure 4a and b). CdS QDs are known to be a transparent window against the sunlight with a wavelength around ∼550 nm because of its wide band gap of ∼2.4−4 eV depending on its dimension. Considering its size of ∼8 nm used here (Figure S2 in SI), it can be more transparent due to quantum confinement effects.[19,20] On the other hand, CdTe QDs have a narrower band gap of ∼1.45 eV[21] and have served as the light absorption layer.[22] The absorbed photons generate electrons and holes in the conduction and valence bands of CdTe QDs, respectively. Due to the established built-in potential at the interface of the CdTe/CdS pn-junction, electrons and holes are forced to be separated completely and accumulated in CdS and CdTe QDs, respectively. A difference in Fermi levels at the two electrodes will drive the accumulated electrons in CdS QDs to flow toward the top ITO electrode, while accumulated holes in CdTe flow toward the bottom Au electrode. Therefore, a DC output is created under constant solar illumination.

In case of VING, however, it generates alternating current (AC) output in synch with an external acoustic waveform, as we observed in Figure 3d. Assume that the ZnO NW is under the compressive strain (Figure 4b, red arrow and line). In this case, NWs have an elevated piezopotential near the bottom Au electrode. An elevated inner potential of NWs drives electron flow toward the external load from the bottom Au electrode, with consideration of the presence of a Schottky barrier at the interface.[23] When the NWs are under tensile strain (Figure 4b, blue arrow and line), the polarity of the piezopotential is reversed, which drives electron flow toward the external load from the top ITO electrode.

As a proof of concept, Figure 4c shows the measured current signal with our HC. When the acoustic wave is applied through the bottom Au electrode, we can obtain AC output with a peak-to-peak current of ∼24 nA and voltage of ∼1 mV (see also Figure S3 in SI) scavenged by VING in the HC. AC output can be understood by our explanation previously presented in the band diagram of VING (Figure 4b, lower band diagram). The output power density of VING can be calculated from the AC power ($P = V_{rms}^2/R_{Load}$) divided by the area of the device. First, the output power of VING is directly obtained from the measured voltage drop in an external load with a resistance of ∼0.1 MΩ (see Figure S4 in SI). The measured voltage drop reaches ∼0.5 mV, representing the AC output power density of ∼5 pW/cm^2. To measure the output signal of the SC in the HC structure (see Experimental Methods in SI), we utilized a solar simulator with an air mass 1.5 global (AM 1.5 G). When simulated light illuminated our HC, DC output was observed, as we explained the detailed procedure previously (Figure 4b, upper band diagram). According to the $I-V$ curve under solar simulation (inset in Figure 4c), the short-circuit current I_{SC} and the open-circuit voltage V_{OC} were found to be ∼57 nA and ∼6 mV, respectively. The DC power density from our SC exhibited ∼97 pW/cm^2, with a fill factor of ∼0.29. We also measured the signal from VING under solar illumination to test its UV response, which can affect the output power of the SC in our hybrid device. It was found to be smaller signals compared to signals from SC (see Figure S5 and S6 in SI). Note that the performance of the VING and SC here are not optimum. However, as a proof of our concept, we could obtain the superimposed signal output by applying an acoustic wave concurrently with a sunlight illumination (Figure 4c, yellow area). Concurrent output of SC (DC) and VING (AC) showed the sum-up of the two individual output signals. It indicates that two generators can work individually or simultaneously for harvesting one or two types of energy.

The superimposed AC and DC output signals from the HC can be separated. In this experiment, one capacitor was added right in front of the preamplifier, which allowed AC to pass through it, while the DC output was stored in it. First, the observation of the single AC signal from VING was tested in a capacitor-connected circuit. Four HCs were connected in parallel and showed an AC output of ∼100 nA under acoustic vibration (Figure 4d). The AC signal passed the capacitor and showed almost the same amplitude as that before passing the capacitor (∼3300 μF) (see also Figure S7 in SI). To test the separation of AC and DC outputs, we applied the simulated sunlight together with acoustic vibration to the HC. When simulated sunlight illuminated the device, the generated DC charges started to be accumulated in the capacitor (7−17 s in

DOI: 10.1021/jz101195n | J. Phys. Chem. Lett. 2010, 1, 2929–2935

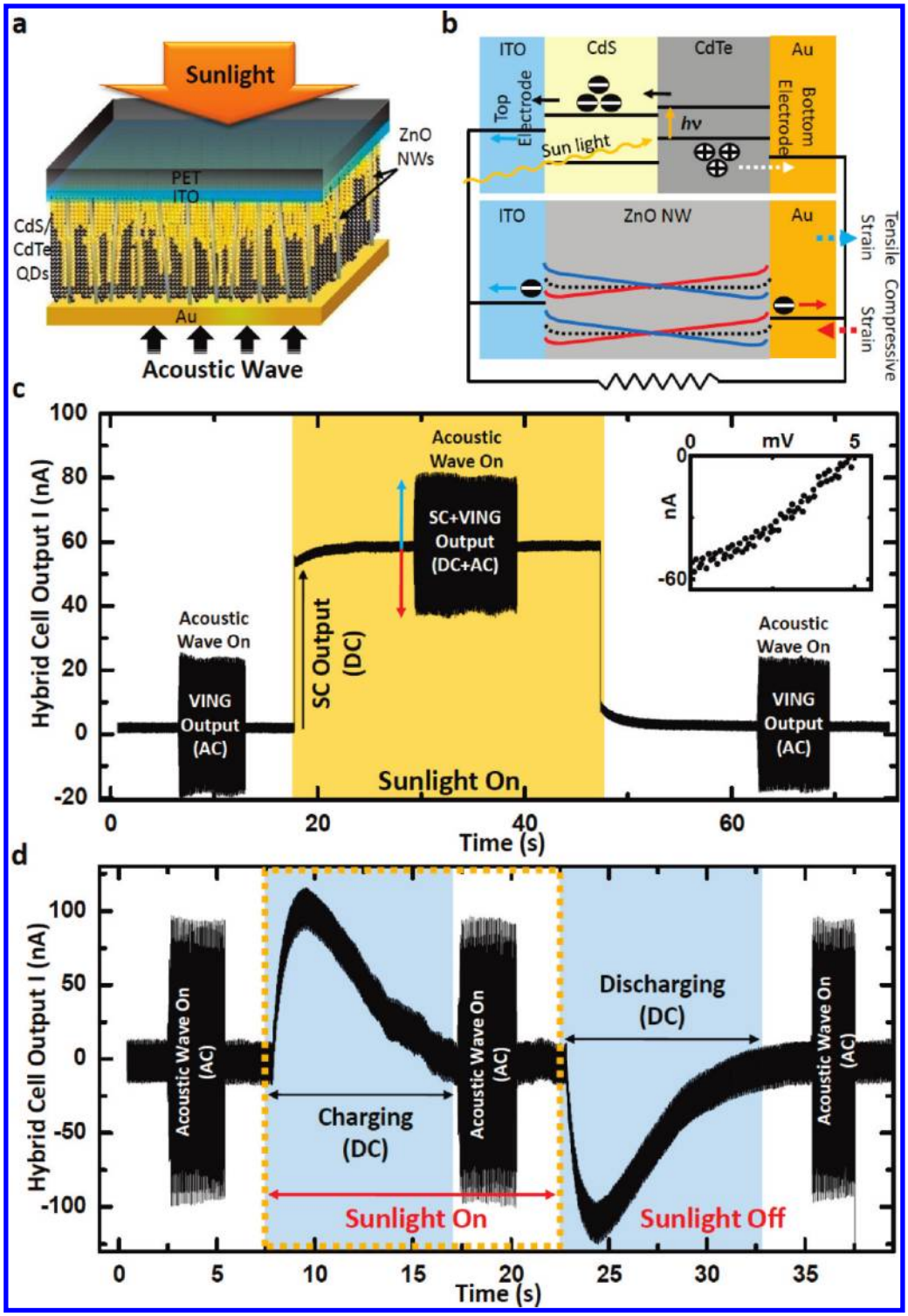

Figure 4. (a) Schematic diagram depicting a hybrid device with two different incoming energy sources. Simulated sunlight illumination and acoustic vibration are delivered through the top PET/ITO layer and the bottom Au electrode, respectively. (b) The energy band diagram of the hybrid device shows electron flows under sunlight illumination and acoustic vibration. Upper and lower schemes correspond to SC and VING, respectively. (c) Short-circuit current output signal of the HC. Acoustic wave applied to the HC before/during/after solar illumination. Inset shows the $I-V$ characteristic of a hybrid device under sunlight illumination. (d) Short-circuit current output signal of the HC after connecting a capacitor right in front of the preamplifier. A capacitor used here for demonstrating the separation of AC and DC output from the HC for their individual applications. From 0 to 7 s, the acoustic wave was on; over 7−17 s, it generated DC by HC and was stored in the capacitor; over 17−22.5 s, it filtered the AC output when the solar part was acting; from 22.5 to 32.5 s, the solar light was turned off resulting in the discharge curve of the capacitor for the stored DC charges; over 32.5−40 s, there was continuous AC output by the acoustic wave when the solar light was off.

DOI: 10.1021/jz101195n | J. Phys. Chem. Lett. 2010, 1, 2929–2935

Figure 4d, first blue area). While the DC power was charging the capacitor, we could obtain clean AC output from VING by the filtering of the capacitor (17−22.5 s in Figure 4d). The separated clean AC signal could be utilized as an energy source to power small electronics, as reported previously.[18] By turning off the simulated sunlight, we observed the discharging curve of the capacitor (22.5−32.5 s in Figure 4d, second blue area). Significantly, this simple demonstration implies that the AC and DC signals from our hybrid cell can be stored individually after their generation by the HC for different applications.

It is important to note that the efficiency of the SC part here is not optimum, but our purpose is to demonstrate an approach for integrating SC and NG into a single device. Our goal is to explore the possible approaches that can achieve HCs. Therefore, in the near future, one can build a more sustainable energy-harvesting system that can harvest energy even in the absence of light.

In summary, we have demonstrated a systematic study of energy conversion using the SWG driven by acoustic vibration in the frequency range of 35 to 1000 Hz, which is the common sound noise in human life. The electricity produced by the SWG is linearly proportional to the input acoustic energy, while the frequency does not affect the performance of the SWG in this study. By infiltrating CdS/CdTe quantum dots among vertical nanowires, we have fabricated a hybrid cell that harvests both sound and solar energies. Since our solar sound generator utilizes the two most common types of energy in our surroundings, it can be a promising approach for driving portable electronics. Furthermore, our composite strategy of NWs and QDs will give an insight into the design of a hybrid device for future applications.

SUPPORTING INFORMATION AVAILABLE Materials for supporting the conclusions and discussions presented in the main text, including the experimental methods, characterization of QDs, voltage, current, and power output, and response of VING and QDs under solar simulation. This material is available free of charge via the Internet at http://pubs.acs.org.

AUTHOR INFORMATION

Corresponding Author:

*To whom correspondence should be addressed. E-mail: zhong.wang@mse.gatech.edu.

Author Contributions:

† These authors contributed equally.

ACKNOWLEDGMENT Research was supported by BES DOE (DE-FG02-07ER46394), NSF (DMS0706436, CMMI 0403671), National Institute For Materials, Japan (Agreement DTD 1 Jul. 2008), and Korea Electronic Technology Institute (KETI). Z.L.W. acknowledges the partial support from the World Class University Program from UNIST, Korea. The authors thank Dr. Yong Ding for his help on TEM characterization of quantum dots.

REFERENCES

(1) Tian, B.; Zheng, X.; Kempa, T. J.; Fang, Y.; Yu, N.; Yu, G.; Huang, J.; Lieber, C. M. Coaxial Silicon Nanowires as Solar Cells and Nanoelectronic Power Sources. *Nature* **2007,** *449*, 885–890.

(2) Wang, Z. L. Self-Powered Nanotech. *Sci. Am.* **2008,** *298*, 82–87.

(3) Dresselhaus, M. S.; Thomas, I. L. Alternative Energy Technologies. *Nature* **2001,** *414*, 332–337.

(4) Wang, Z. L. Towards Self-Powered Nanosyatems: From Nanogenerators to Nanopiezotronics. *Adv. Funct. Mater.* **2008,** *18*, 3553–3567.

(5) Hong, K.-S.; Xu, H.; Konishi, H.; Li, X. Direct Water Splitting Through Vibrating Piezoelectric Microfibers in Water. *J. Phys. Chem. Lett.* **2010,** *1*, 997–1002.

(6) Xu, C.; Wang, X.; Wang, Z. L. Nanowire Structured Hybrid Cell for Concurrently Scavenging Solar and Mechanical Energies. *J. Am. Chem. Soc.* **2009,** *131*, 5866–5872.

(7) Hansen, B. J.; Liu, Y.; Yang, R.; Wang, Z. L. Hybrid Nanogenerator for Concurrently Harvesting Biomechanical and Biochemical Energy. *ACS Nano* **2010,** *4*, 3647–3652.

(8) Wang, X.; Song, J.; Liu, J.; Wang, Z. L. Direct-Current Nanogenerator Driven by Ultrasonic Waves. *Science* **2007,** *316*, 102–105.

(9) Yang, R.; Qin, Y.; Dai, L.; Wang, Z. L. Power Generation with Laterally-Packaged Piezoelectric Fine Wires. *Nat. Nanotechnol.* **2009,** *4*, 34–39.

(10) Yang, R.; Qin, Y.; Li, C.; Zhu, G.; Wang, Z. L. Converting Biomechanical Energy into Electricity by a Muscle-Movement-Driven Nanogenerator. *Nano Lett.* **2009,** *9*, 1201–1205.

(11) Gur, I.; Fromer, N. A.; Geier, M. L.; Alivisatos, A. P. Air-Stable All-Inorganic Nanocrystal Solar Cells Processed from Solution. *Science* **2005,** *310*, 462–465.

(12) Roundy, S.; Leland, E. S.; Baker, J.; Carleton, E.; Reilly, E.; Lai, E.; Otis, B.; Rabaey, J. M.; Wright, P. K.; Sundararajan, V. Improving Power Output for Vibration-based Energy Scavengers. *IEEE Pervas. Comput.* **2005,** *4*, 28–36.

(13) Wang, Z. L.; Song, J. Piezoelectric Nanogenerators Based on Zinc Oxide Nanowire Arrays. *Science* **2006,** *312*, 242–246.

(14) Wang, X.; Liu, J.; Song, J.; Wang, Z. L. Integrated Nanogenerators in Biofluid. *Nano Lett.* **2007,** *7*, 2475–2479.

(15) Qin, Y.; Wang, X.; Wang, Z. L. Microfibre−Nanowire Hybrid Structure for Energy Scavenging. *Nature* **2008,** *451*, 809–813.

(16) Vayssieres, L. Growth of Arrayed Nanorods and Nanowires of ZnO from Aqueous Solutions. *Adv. Mater.* **2003,** *15*, 464–466.

(17) Yang, R.; Qin, Y.; Li, C; Dai, L.; Wang, Z. L. Characteristics of Output Voltage and Current of Integrated Nanogenerators. *Appl. Phys. Lett.* **2009,** *94*, 022905.

(18) Xu, S.; Qin, Y.; Xu, C.; Wei, Y.; Yang, R.; Wang, Z. L. Self-Powered Nanowire Devices. *Nat. Nanotechnol.* **2010,** *5*, 366–373.

(19) Singh, V. P.; Singh, R. S.; Thompson, G. W.; Jayaraman, V.; Sanagapalli, S.; Rangari, V. K. Characteristics of Nanocrystalline CdS Films Fabricated by Sonochemical, Microwave and Solution Growth Methods for Solar Cell Applications. *Sol. Energy Mater. Sol. Cells* **2004,** *81*, 293–303.

(20) Alivisatos, A. P. Perspectives on the Physical Chemistry of Semiconductor Nanocrystals. *J. Phys. Chem.* **1996,** *100*, 13226–13239.

(21) Britt, J.; Ferekides, C. Thin-Film CdS/CdTe Solar Cell with 15.8% Efficiency. *Appl. Phys. Lett.* **1993,** *62*, 2851–2852.

(22) Singh, V. P.; McClure, J.; Lush, G. B.; Wang, W.; Wang, X.; Thompson, G. W.; Clark, E. Thin Film CdTe−CdS Heterojunction Solar Cells on Lightweight Metal Substrates. *Sol. Energy Mater. Sol. Cells* **1999,** *59*, 145–161.

(23) Wang, Z. L. Piezotronic and Piezophototronic Effects. *J. Phys. Chem. Lett.* **2010,** *1*, 1388–1393.